Supporting Information

Title: Joint Tuning of Nanostructured Cu-Oxide Morphology and Local Electrolyte Programs High-Rate CO_2 Reduction to C_2H_4

Yuanjie Pang[1†], Thomas Burdyny[1†], Cao-Thang Dinh[2], Md Golam Kibria[2], James Zhangming Fan[2], Min Liu[2], Edward H. Sargent[2*], and David Sinton[1*]

[†]These authors contributed equally to this work.

Modeling of the Diffusion Region and Surface Mass Transport

The modeling results throughout the manuscript were performed as detailed in our previous manuscript[1] and are briefly summarized here. All simulations were performed in 1D in MATLAB. The diffusion region consisted of a left-hand boundary (x = 0 μm) consisting of the electrode surface and a right-hand boundary at the edge of the diffusion layer (x = δ) where the concentrations of all aqueous components are assumed to be equal to their bulk concentrations depending on the concentration of electrolyte used.

The thickness of the diffusion layer, δ, was determined as described previously where the thickness varies depending on the electrode current density, product selectivity and the size distribution of product bubbles evolving from the electrode. Taken into account gas evolution is needed as the mass transport invoked by bubble growth and departure is larger than that of a stirred beaker at even moderate electrode current densities. Within the simulation, current densities are prescribed and the bubble size distribution is taken directly from the experimentally measured values for each electrode shown in Figure 1 f-j. The diffusion thickness can then be calculated as a function of current density, selectivity and electrode choice and results in the variations between electrodes observed in Figure 2.

The diffusion region itself was modeled similar to other sources with the exception of the varying diffusion thickness.[2] Taken into account are the interactions between CO_2 and the carbonate electrolyte, 'salting out' effects of CO_2 in a salt solution, OH generation at the electrode surface and CO_2 consumption at the electrode as a function of current density. The following equations are subsequently solved to determine the local pH and CO_2 concentration at the electrode's surface:

$$\frac{\partial[CO_2]}{\partial t} = D_{CO_2}\frac{\partial^2[CO_2]}{\partial x^2} - [CO_2][OH^-]k_{1f} + [HCO_3^-]k_{1r}$$

(1)

$$\frac{\partial[HCO_3^-]}{\partial t} = D_{HCO_3^-}\frac{\partial^2[HCO_3^-]}{\partial x^2} + [CO_2][OH^-]k_{1f} - [HCO_3^-]k_{1r} - [HCO_3^-][OH^-]k_{2f} + [CO_3^{2-}]k_{2r}$$

(2)

$$\frac{\partial[CO_3^{2-}]}{\partial t} = D_{CO_3^{2-}}\frac{\partial^2[CO_3^{2-}]}{\partial x^2} + [HCO_3^-][OH^-]k_{2f} - [CO_3^{2-}]k_{2r}$$

(3)

$$\frac{\partial[OH^-]}{\partial t} = D_{OH^-}\frac{\partial^2[OH^-]}{\partial x^2} - [CO_2][OH^-]k_{1f} + [HCO_3^-]k_{1r} - [HCO_3^-][OH^-]k_{2f} + [CO_3^{2-}]k_{2r}$$

(4)

Rate constants of the carbonate equilibrium are calculated as a function of temperature and salinity[3] while the 'salting out' effect is calculated from the Sechenov equation.[4]

The right-hand boundary conditions set the CO_2, HCO_3^-, CO_3^{2-} and OH^- concentrations equal to their bulk concentrations, depending on the $KHCO_3$ concentration used in the experiments. This assumes the H-cell beaker is well mixed with saturated CO_2 at the 500 rpm stirring speed and CO_2 headspace as described in the Experimental Section.

At the left boundary the flux of CO_2 and OH^- were fixed to the applied current density and chosen selectivity. The local pH at the electrode then increases with the applied current density while the amount of CO_2 consumed increases.

Figure S1. Cyclic voltammograms of the Flat and Porous samples (a) Flat, (b) Porous 1, (c) Porous 2, (d) Porous 3, (e) Porous 4. (f) Corresponding charging current density differences ($\Delta J = j_a - j_c$) plotted against scan rates. CV scans are performed in 0.1 M $KHCO_3$ saturated with CO_2.
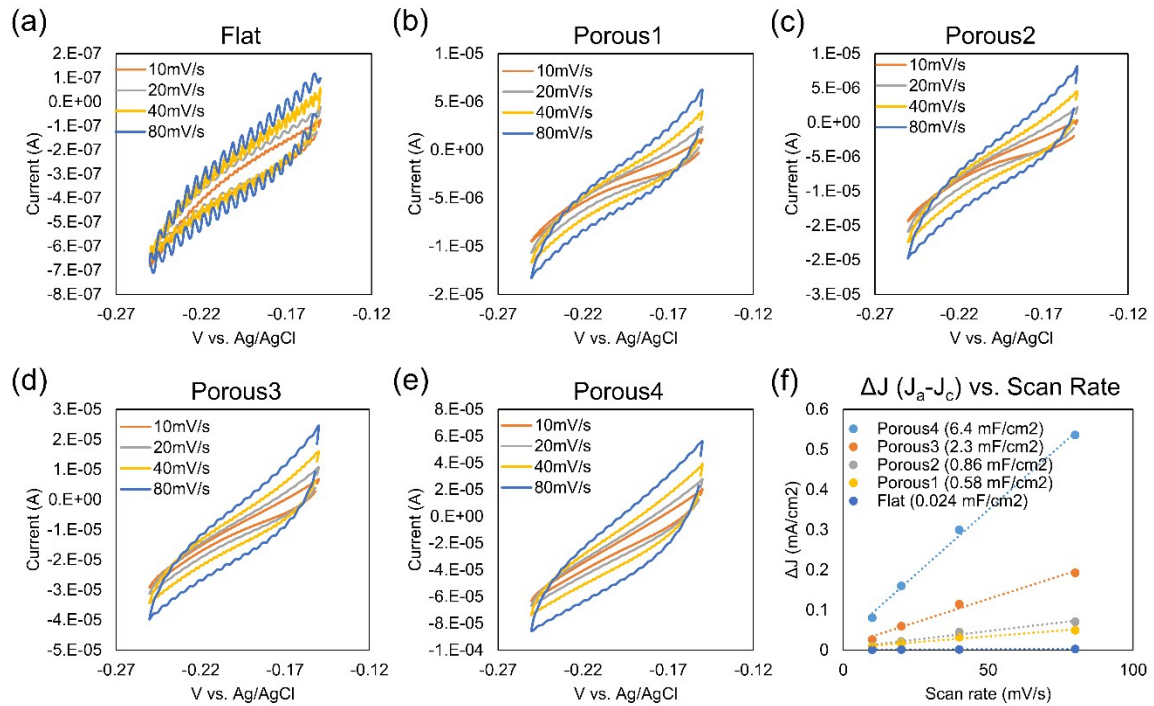
Figure S2. Under potential deposition of Pb onto the Flat and Porous samples to quantify the electrochemically active surface area. (a) Cyclic voltammetry measurements in an aqueous electrolyte containing 0.01 M Pb(NO$_3$)$_2$ and 0.1 M HCl. (b) Normalized active surface area for each sample versus the Flat sample.
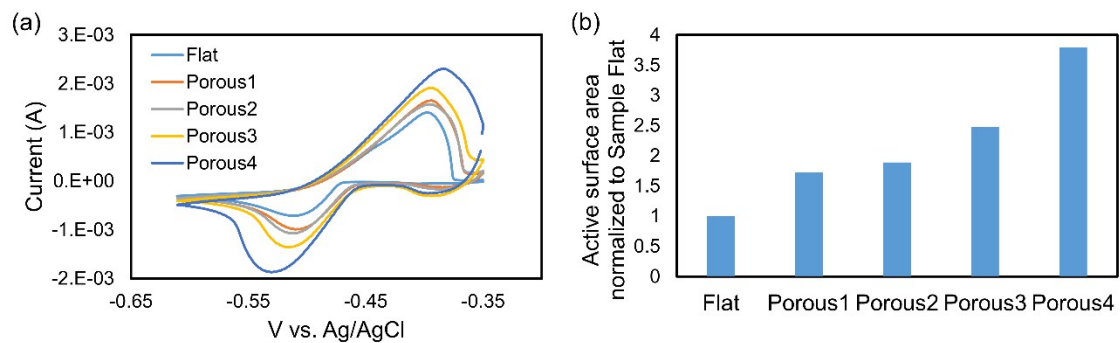
Figure S3. XPS spectral characterization of the Flat and Porous samples before and after CO2RR. (a) Flat sample, (b) Porous1 sample, (c) Porous2 sample, (d) Porous3 sample, (e) Porous4 sample, (f) Peak positions of the Cu 2p3/2 peak before and after CO_2RR for all samples.
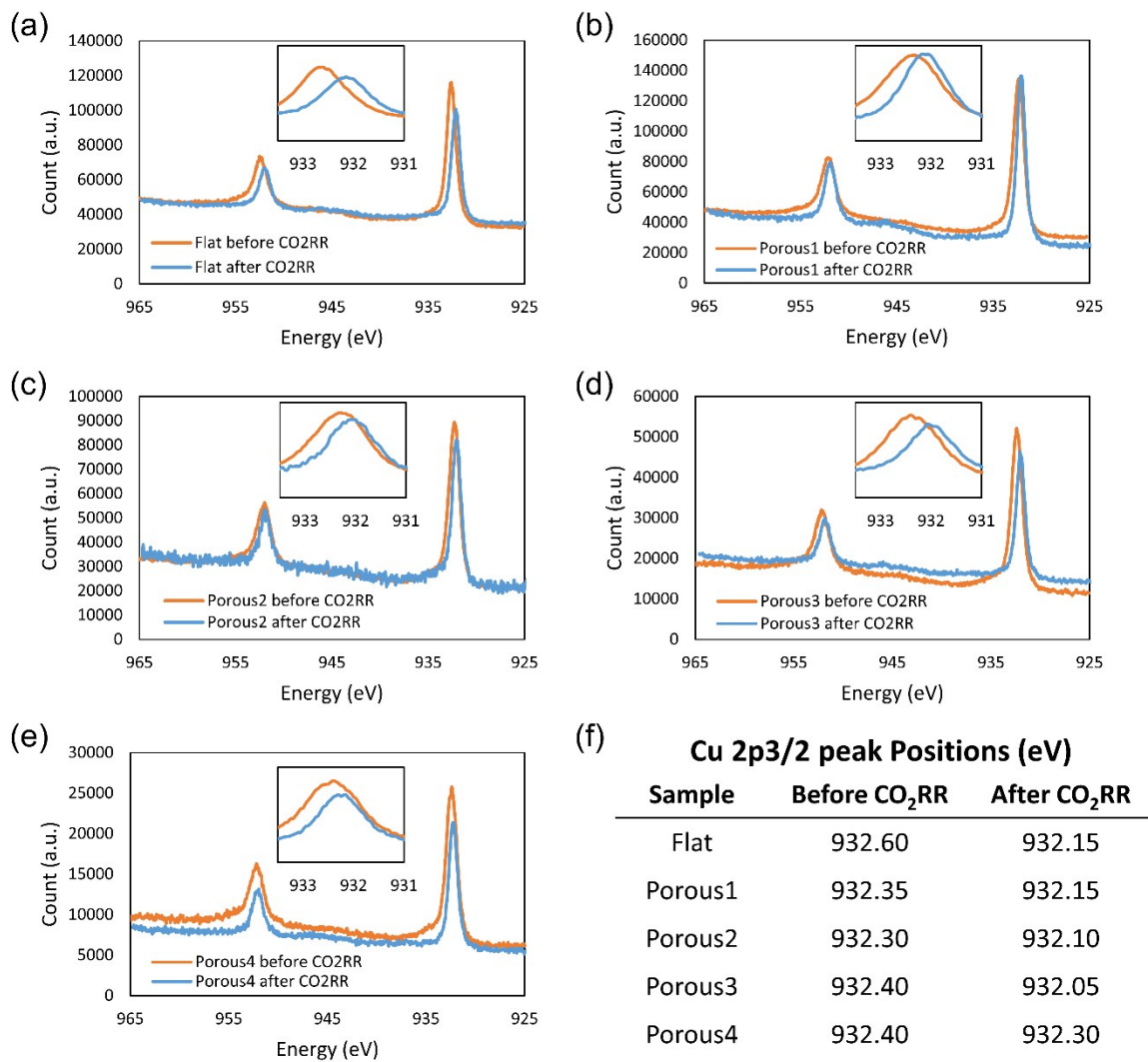

(f)

Cu 2p3/2 peak Positions (eV)

Sample	Before CO_2RR	After CO_2RR
Flat	932.60	932.15
Porous1	932.35	932.15
Porous2	932.30	932.10
Porous3	932.40	932.05
Porous4	932.40	932.30

Figure S4. SEM images of Cu-based catalysts. (a-c) Flat samples. (d-o) Samples based on electrodeposition of porous Cu structures with various deposition duration of 2 s (d-f), 4 s (g-i), 8 s (j-l), and 16 s (n-o). Panels (a, d, g, j, and n) show samples before wet-oxidation; Panels (b, e, h, k, and l) show samples after wet-oxidation; Panels (b, e, h, k, and l) show samples after CO2RR for 30 minutes. All scale bars represent 20 μm.
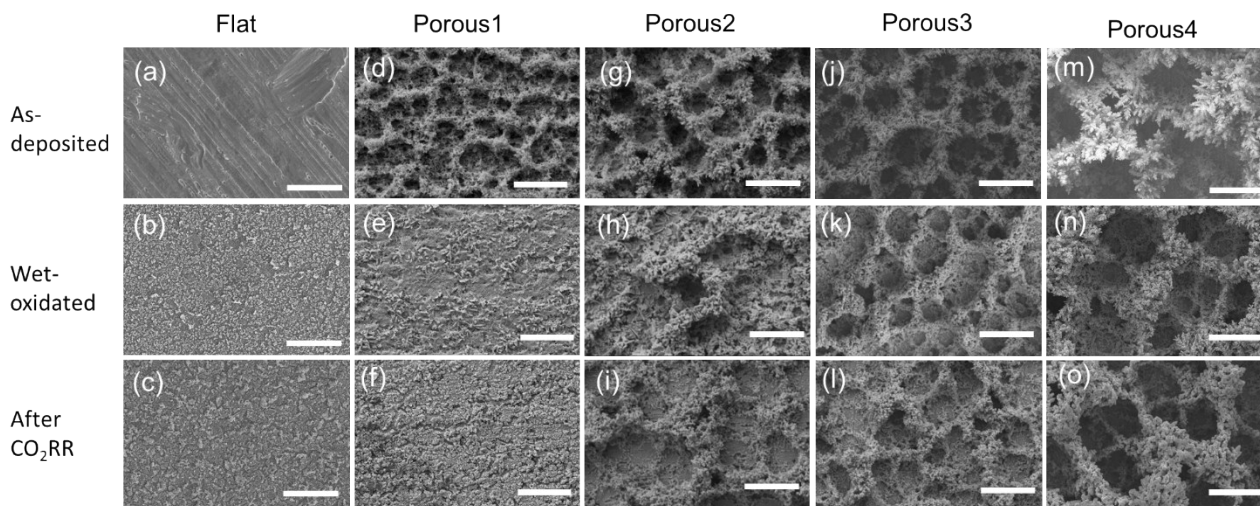
Figure S5. Ethylene production rate versus total current density at 0.1 M, 0.2 M, 0.3 M and 0.5 M KHCO$_3$ concentrations for the Flat electrode.
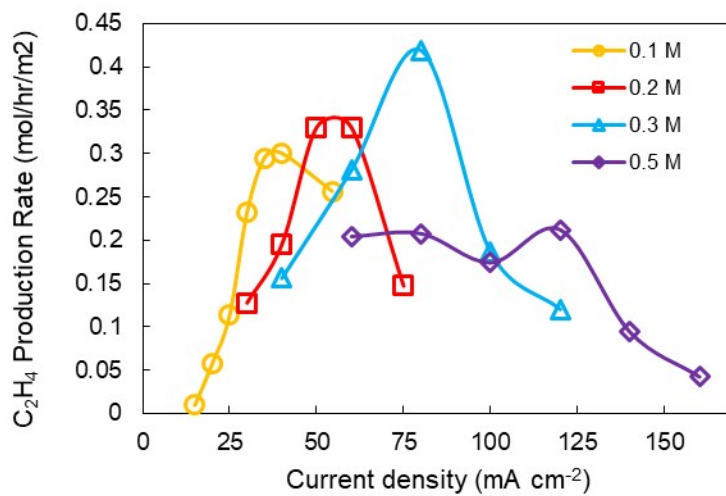
Figure S6. Ethylene production rate versus total current density at 0.1 M, 0.2 M, 0.3 M and 0.5 M KHCO$_3$ concentrations for the Flat electrode.
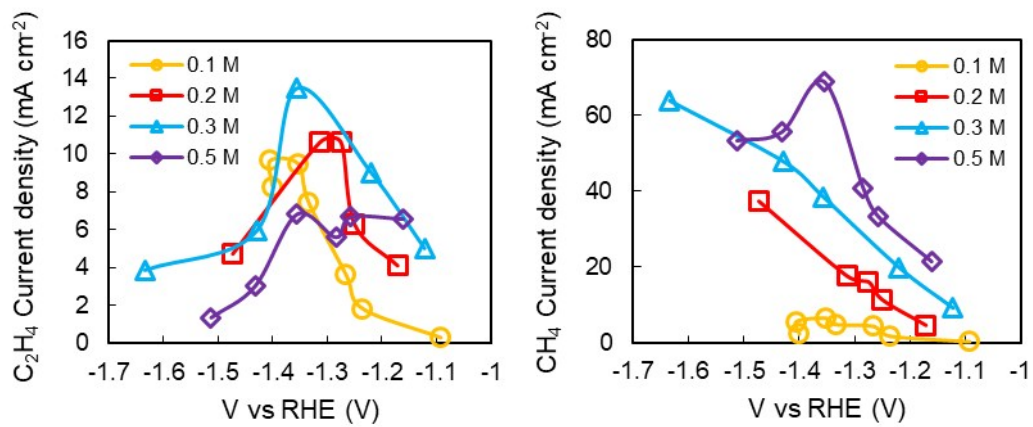
Figure S7. Stability test of the electrocatalyst tested using Sample Porous 2, 0.1 M KHCO$_3$, 50 mA cm^{-2} total current.
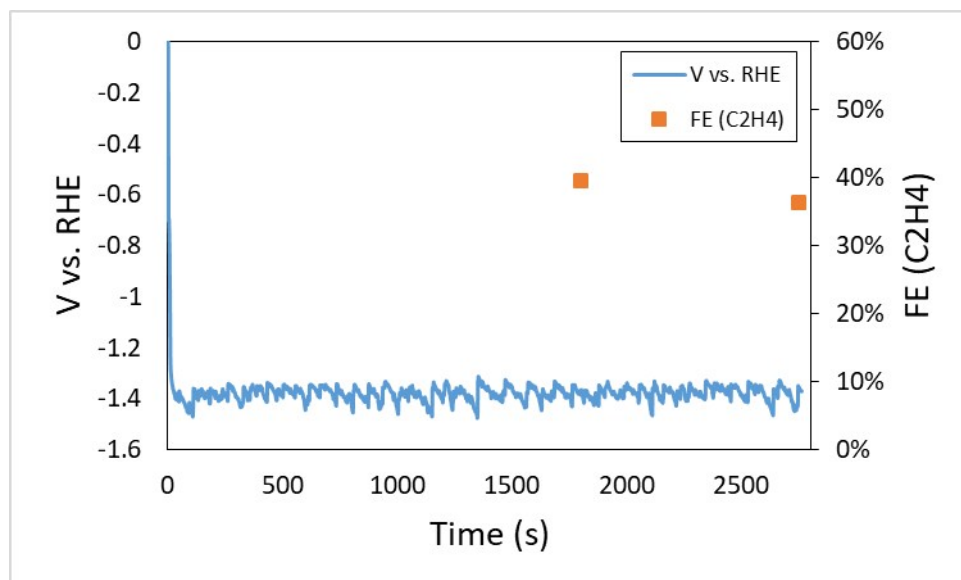
Figure S8. Total current density versus applied potential for 0.1 M KHCO₃ concentrations for the Porous electrode samples.
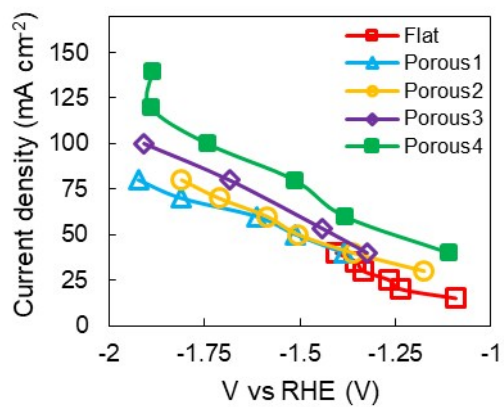
Figure S9. Tafel plots for target products. (a) Ethylene current density versus potential in 0.1 M KHCO₃, (b) Methane current density versus potential in 0.1 M KHCO₃, (c) Ethylene current density versus potential in 0.2 M KHCO₃, (d) Methane current density versus potential in 0.2 M KHCO₃.
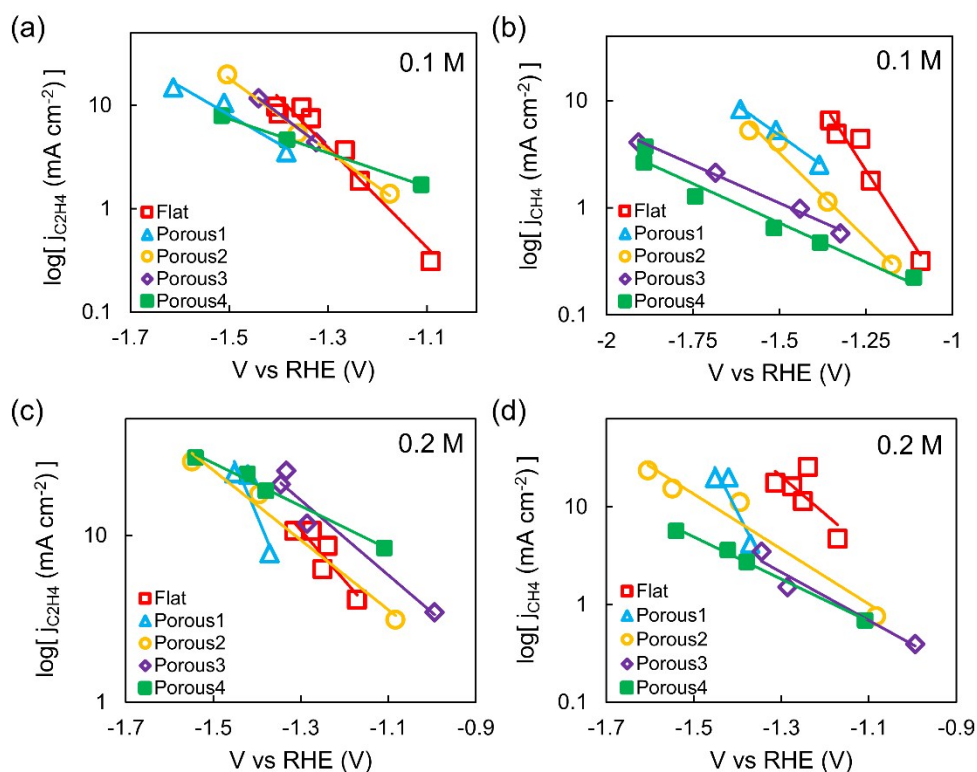

Table S1. Tafel slopes for the target products, C_2H_4 and CH_4, for all samples in 0.1 M and 0.2 M KHCO₃

	Tafel Slopes (mV dec⁻¹)			
	0.1 M		0.2 M	
	C_2H_4	CH_4	C_2H_4	CH_4
Flat	207	199	331	260
Porous 1	361	439	159	113
Porous 2	287	315	478	271
Porous 3	275	701	445	405
Porous 4	608	682	776	462

Figure S10. XRD characterization pattern of the wet-oxidated Cu foil, showing signals from the Cu substrate and a surface layer of various forms of Cu oxides, with a majority of Cu_2O and a minority of other types of oxides.
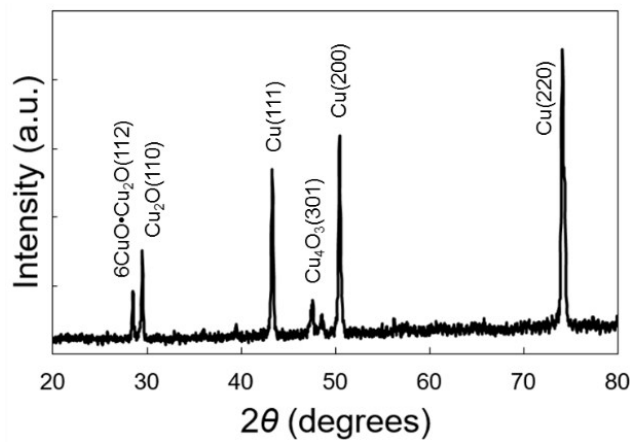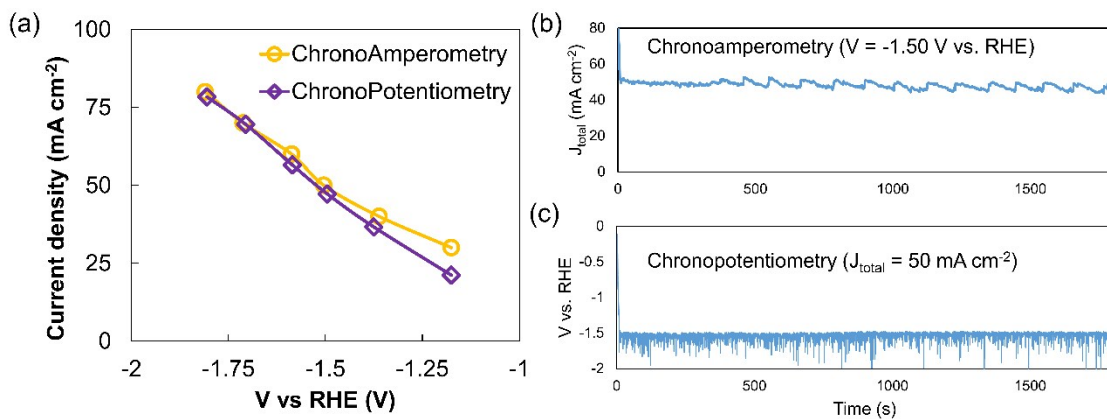
Figure S11. (a) Comparison of chronoamperometry and chronopotentiometry measurements for 6 points on a Porous 2 sample in 0.1 M KHCO$_3$. (b) Chronoamperometry measurement at -1.5 V vs RHE for 1800s. (c) Chronopotentiometry measurement at 50 mA cm^{-2} for 1800s.

Supplementary References

[1] T. Burdyny, P. J. Graham, Y. Pang, C.-T. Dinh, M. Liu, E. H. Sargent, D. Sinton, *ACS Sustain. Chem. Eng.* **2017**, DOI 10.1021/acssuschemeng.7b00023.

[2] M. R. Singh, E. L. Clark, A. T. Bell, *Phys. Chem. Chem. Phys.* **2015**, *17*, 18924–18936.

[3] F. J. Millero, T. B. Graham, F. Huang, H. Bustos-Serrano, D. Pierrot, *Mar. Chem.* **2006**, *100*, 80–94.

[4] S. Weisenberger, A. Schumpe, *AIChE J.* **1996**, *42*, 298–300.

[5] D. Tahir, S. Tougaard, *J. Phys. Condens. Matter* **2012**, *24*, 175002.